Hole motion in a quantum Néel state

Subir Sachdev
Center for Theoretical Physics, P.O. Box 6666, Yale University, New Haven, Connecticut 06511
(Received 22 April 1988)

The spin-wave expansion is used to motivate a simple trial wave function for the Néel ground state of a spin-$\frac{1}{2}$ Heisenberg antiferromagnet on a square lattice; the wave function yields an upper bound on the ground-state energy per bond of $(-0.3317\pm0.0002)J$, where J is the exchange constant. The wave function is easily generalizable to the case where a single hole, with hopping matrix element t, is present. The hole energy-momentum relationship is determined for $J/t>0.25$; the minimum hole energy is always on the zone boundary at $\mathbf{k}=(\pi/2,\pi/2)$. The hole bandwidth, W, has a maximum value of $1.24t$ at $J=0.73t$. The small parameter which makes all of these calculations possible is $1/(2Z-2)$, where $Z=4$ is the coordination number of the square lattice.

I. INTRODUCTION

Highly correlated lattice electron systems, especially those close to half-filling, are the subject of intense current theoretical interest. This interest was stimulated in part by the discovery of high-temperature superconductivity in La_2CuO_4 and related compounds.[1] These systems are also of theoretical interest in their own right, with a large number of fascinating theoretical questions remaining unanswered.[2] This paper investigates the properties of two such systems—(i) the spin-$\frac{1}{2}$ Heisenberg antiferromagnet, with nearest-neighbor exchange constant J, on a two-dimensional square lattice, and (ii) the spin-$\frac{1}{2}$ Heisenberg antiferromagnet with one spin removed; this vacancy or hole can hop through the lattice with a nearest-neighbor hopping matrix element t. The spin configurations in both cases will be assumed to possess long-range Néel order. The main result of this paper will be a variational determination of the energy-momentum relationship of a single hole moving in a background quantum Néel state for a wide range of values of the ratio J/t.

Motivation for the problems investigated in this paper is provided by several recent experimental and theoretical investigations. Neutron scattering[3] on undoped La_2CuO_4 revealed the existence of long-range three-dimensional Néel order and a large two-dimensional spin correlation length. A subsequent theoretical analysis[4] has convincingly argued that the neutron scattering experiments indicate the presence of long-range *two-dimensional* Néel order at zero temperature. Two independent Monte Carlo simulations[5,6] of the nearest neighbor spin-$\frac{1}{2}$ Heisenberg antiferromagnet on a square lattice are consistent with the existence of long-range Néel order in the ground state. In this paper we will discuss a simple trial wave function which provides a reasonable characterization of this long-range ordered ground state and the ground-state correlation functions. Low-order calculations on a similar, but not identical, wave function were performed by Fisher[7] and Eguchi.[8] The chief utility of our variational state is however that it is straightforwardly generalizable to the more interesting problem of the Heisenberg antiferromagnet with a single hole. A proper determination of the properties of a single hole is clearly necessary in the understanding of the properties of a many hole system and the possible existence of high-temperature superconductivity in a purely repulsive single-band Hubbard model.

We begin with a brief presentation of the results of the analysis of the spin-$\frac{1}{2}$ Heisenberg antiferromagnet. The system is described by the

$$H_{\rm AF}=J\sum_{i\in A}\sum_{j\in i+\delta}\mathbf{S}^a(i)\cdot\mathbf{S}^b(j)\ , \tag{1.1}$$

where the $\mathbf{S}^{a,b}$ are spin-$\frac{1}{2}$ operators, the sum over i extends over the A sublattice of the square lattice, and j lies on the B sublattice and is restricted to be one of the nearest neighbors of i. Conventional large-S expansion methods can be used to show that the leading $1/S$ prediction for the ground state of $H_{\rm AF}$ is very closely approximated by the state $|\Psi\rangle$:

$$|\Psi\rangle=\prod_{i\in A}\prod_{j\in i+\delta}[1-g\sigma^a_-(i)\sigma^b_+(j)]|0\rangle\ , \tag{1.2}$$

where $|0\rangle$ is the classical Néel state with all spins up on sublattice A and all spins down on sublattice B, and σ^a_- are the usual Pauli matrices on the two sublattices. The possibility that $|\Psi\rangle$ may be a reasonable trial wave function for the antiferromagnet was suggested to the author by C. M. Varma.[9] The large-S expansion yields a value for the parameter g of 0.36 in $d=1$ and 0.16 in $d=2$. Recent studies[5,6,10] have indicated that the large-S expansion is remarkably accurate in determining the ground-state energy and the sublattice magnetization of $H_{\rm AF}$. We may therefore treat the state $|\Psi\rangle$ as a good variational guess for the ground state $H_{\rm AF}$ with g treated as a *free* variational parameter.

Exact evaluation of the expectation value of $H_{\rm AF}$ in the state $|\Psi\rangle$ is only possible in one dimension. This calculation is presented in Sec. II A and yields a minimum value of the energy per bond of $-0.428J$ at $g=0.389$. This compares reasonably with the exact ground-state energy

 ©1989 The American Physical Society

of $-0.443J$. The sublattice magnetization at this value of g is calculated to be 0.289 (in units where the classical magnetization is 0.5), whereas the exact ground state has no long-range order. There exist other trial wave functions which yield lower energies and sublattice magnetizations than $|\Psi\rangle$.[5] The properties of $|\Psi\rangle$ are much more encouraging in two dimensions, where the quantum fluctuations from the classical Néel state are expected to be smaller. As an exact evaluation of the ground-state energy is no longer possible, we develop a renormalized self-consistent expansion in the parameter g which allows determination of the expectation value of $H_{\rm AF}$ to better than 0.2%. This expansion is based upon a mapping of the problem to the statistical mechanics of monomers, dimers, and loops upon the square lattice; this statistical mechanical problem is in turn mapped onto a Grassmannian functional integral which is then evaluated in a self-consistent perturbation theory in g^2. One reason for the accuracy of this procedure is that g is quite small in $d=2$. The large-S theory predicts a value of 0.16. In addition, a straightforward evaluation of the expectation value of $H_{\rm AF}$ to second order in g yields the result

$$g \approx \frac{1}{2Z-2} , \tag{1.3}$$

where $Z=4$ is the coordination of the square lattice. The renormalized perturbation expansion in g converges very quickly and yields a variational upper bound for the ground-state energy of $H_{\rm AF}$ of $(-0.3317\pm0.0002)J$. This compares favorably with the estimate of $(-0.334\pm0.001)J$ made by Huse using series expansions.[5] It is also the lowest upper bound among existing variational calculations with a *single* variational parameter.[5,11]

We now turn to the problem of a single vacancy in an antiferromagnet. The system is described by the Hamiltonian H_h,

$$H_h = -t \sum_{i\in A} \sum_{j\in i+\delta} (c^\dagger_{i\alpha} c_{j\alpha} + \text{H.c.}) + J \sum_{i\in A} \sum_{j\in i+\delta} \mathbf{S}^a(i)\cdot\mathbf{S}^b(j) , \tag{1.4}$$

where $c_{i,\alpha}$ are the usual fermeon operators and

$$S_\mu(i) = \tfrac{1}{2} c^\dagger_{i\alpha} \sigma^\mu_{\alpha\beta} c_{i\beta} ;$$

there is also a restriction forbidding double occupancy of every site. We will restrict our attention to the section of the Hilbert space with the number of electrons equal to one less than the number of sites in the system. The Hamiltonian H_h can be obtained as the effective Hamiltonian describing the large U limit of the Hubbard model (where U is the repulsion between two electrons on the same site) after states containing more than one electron per site have been eliminated[12] (a "pair-hopping" term which can cause a hole to hop to a second-nearest-neighbor site has been omitted). The derivation of H_h from the Hubbard model always yields $J/t \ll 1$; however, this regime of parameters is the most intractable and we shall find it convenient to treat J/t as a free parameter and deduce properties of the $J/t \ll 1$ limit from insight gained from the large J/t regime. The properties of H_h (with the "pair-hopping" term included) were recently investigated numerically by Trugman[13] by exact diagonalization on a truncated Hilbert space. The variational method of this paper uses instead a Jastrow-type wave function (see the following) which is chosen to properly account for the distortion of the Néel order around the hole. After the work described in this paper had been completed and the paper written, the author learned of the work of Shraiman and Siggia,[14] Kane *et al.*,[15] and Schmitt-Rink,[16] all of which addressed the properties of H_h (with the "pair-hopping" term excluded). The results of these investigators and the present work are in qualitative agreement (see the following).

We shall describe the properties of the hole in the antiferromagnet by variational states which are a simple generalization of the state $|\Psi\rangle$ used to describe the quantum Néel state. These variational states can be written in the form

$$|\mathbf{R};\mathcal{F}\rangle = \frac{1}{K} \prod_{i,j\text{NN}}{}' [1 - G(i,j)\sigma^a_-(i)\sigma^b_+(j)] |\mathbf{R}^0;\mathcal{F}\rangle , \tag{1.5}$$

where $|\mathbf{R}^0;\mathcal{F}\rangle$ is a classical Néel state with a hole at $\mathbf{R}$ and a few (≤ 5) spins flipped with respect to the Néel state, $\mathcal{F}$ is a label for the set of flipped spins, K is a normalization constant, the $G(i,j)$ are an infinite set of variational parameters, and the product extends over a restricted set of bonds which do not touch either the hole site or the flipped spins in the set $\mathcal{F}$. An important constraint which must be satisfied for the states in Eq. (1.5) to be reasonable trial wave functions for the ground state of H_h, is that *the absolute values of the set of variational parameters $G(k,j)$ must be much smaller than unity at the minimum energy.* This follows from the procedure used in motivating the state $|\Psi\rangle$: only if each bond has a small amplitude for flipping the spins at its ends, will the neglect of longer-range bonds be reasonable. The parameter which makes this amplitude small is essentially the inverse of the coordination number of the bond, $1/(2Z-2)$. We will show in the body of the paper that with a careful choice of 13 different sets of flipped spins $\mathcal{F}$, we are able to satisfy $|G(i,j)|<0.5$ for all $J/t>0.25$. The procedure for determining the energy of the hole therefore involves writing down eigenstates of momentum by combining the states in Eq. (1.5) into plane-wave states; the Hamiltonian can then be expressed as a 13×13 matrix which is then diagonalized. Note that the variational parameters $G(i,j)$ will be a function of the momentum $\mathbf{k}$ and will not be invariant under the symmetry group of the square lattice. Also, the matrix elements of this Hamiltonian are only determined to second order in $G(i,j)$; our experience with $H_{\rm AF}$ indicates this to be a good approximation. The arguments presented earlier and in Section III B lead to the following conclusions on the usefulness of the states in Eq. (1.5): (i) The small values of $|G(i,j)|$ at the minimum energy indicates that the states $|\mathbf{R};\mathcal{F}\rangle$ with 13 different sets of flipped spins $\mathcal{F}$ are a good variational basis set for all $J/t>0.25$. (ii) The smallness of $|G(i,j)|$ also allows evaluation of the bandwidth of the hole within an accuracy of 9% for $J/t=1$,

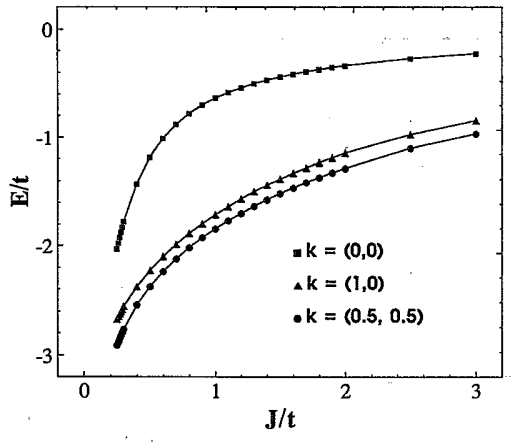

FIG. 1. The energy of a hole E moving with hopping matrix element t moving in a Néel state with exchange constant J. The zero of energy is the ground-state energy of the antiferromagnet with *one hole* and $t=0$. The energy is plotted at the three momenta $\mathbf{k}=(0,0)$, $\mathbf{k}=(\pi,0)$, and $(\pi/2,\pi/2)$. The momenta have been labeled in units of π in the figure.

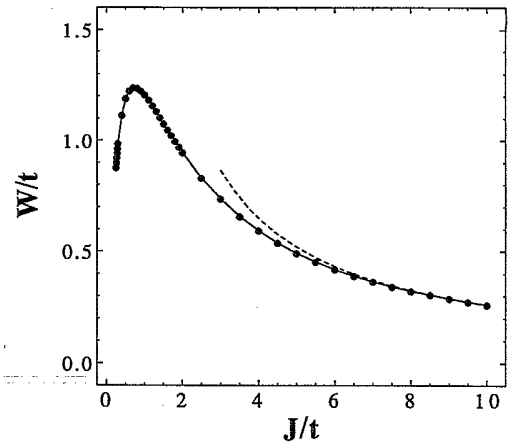

FIG. 2. The hole bandwidth $W/t=E/t(\mathbf{k}=(0,0))-E/t(\mathbf{k}=(\pi/2,\pi/2))$ as a function of J/t. The dashed line is the best fit to the functional form $W\approx ct^2/J$ at the value of $c=2.6$.

and within an accuracy of 25% for $J/t=0.25$.

The results of the calculation are summarized in Figs. 1 and 2, which are the central results of this paper. Figure 1 shows the energy of the hole E/t at the three different momenta $(0,0)$, $(\pi,0)$, and $(\pi/2,\pi/2)$ as a function of J/t. The zero of energy is the energy of the antiferromagnet with *one hole* and $t=0$. For all values of J/t, the global minimum state is always at the momentum $(\pi/2,\pi/2)$. This feature was also present in the calculations of Shraiman and Siggia[17] and Trugman.[13] Direct numerical comparison of our results with those of Trugman is not possible because the Hamiltonian considered by him is not identical to ours; using $J=4t^2/U$, we find the energy of the $\mathbf{k}=(0,0)$ state to be within 15% of the results of Trugman in the $J/t<1$ regime. However, we find that the energies of the $\mathbf{k}=(\pi,0)$ and the $\mathbf{k}=(\pi/2,\pi/2)$ states decrease as J/t decreases below $J/t=1$, while Trugman finds that the energies increase with decreasing J/t. We show in Fig. 2 the bandwidth of the hole

$$W/t=E/t(\mathbf{k}=(0.0))-E/t(\mathbf{k}=(\pi/2,\pi/2))\ .$$

A remarkable feature of this figure is the *maximum* in the bandwidth at $J=0.73t$ where $W=1.24t$. At large values of J/t we find $W\approx 2.6t^2/J$; this feature can also be understood from a large J/t perturbation theory for the hole. The dashed line in Fig. 2 shows the best fit to this functional form. For small values of J/t, the bandwidth satisfies $W\approx 3.4J$. This linear decrease in the band width W with J is consistent with the results of Schmitt-Rink *et al.*,[16] Kane *et al.*,[15] and Shraiman and Siggia.[17,14] Kane *et al.* have also argued that the decrease in W is consistent with the enhancement of the hole mass observed in optical absorption experiments.[18]

The outline of the rest of the paper is as follows. Section II deals with the properties of the spin-$\frac{1}{2}$ Heisenberg antiferromagnet in two subsections: (i) the first subsection presents exact evaluation of the variational wave function in one dimension and (ii) the second subsection deals with the properties of the two-dimensional antiferromagnet. Intermediate steps in the evaluation of the variational energy using the monomer-dimer-loop counting problem and the Grassmann functional integral are relegated to Appendix A. Section III evaluates the energy of a single hole. Two different trial wave functions are used. The first, discussed in Sec. III A, is simpler, but is useful only for $J/t\gg 1$. The failures of this simple wave function help motivate the second more complex wave function discussed in Sec. III B. The results summarized in this Introduction were obtained using the second wave function. Some details in the evaluation of the matrix elements of the H_h are discussed in Appendix B. The conclusion contains a brief discussion of other problems that may be attacked using the approach of this paper.

II. ANTIFERROMAGNET WITHOUT HOLES

We begin by establishing notation with a brief review of the Holstein-Primakoff[19] transformation for generating a large-S expansion for the Heisenberg antiferromagnet. The transformation introduces a mapping between the Hilbert space of the spins and the Hilbert space of two species of bosons. The bosons are created by the operators $a_i^\dagger$ and $b_i^\dagger$ and represent spin flips on sublattices A and B, respectively. The correspondence between the operators is given by

$$S_+^a(i)=\sqrt{2S}\left[1-\frac{a_i^\dagger a_i}{2S}\right]^{1/2}a_i;\ S_-^a(i)=\sqrt{2S}\,a_i^\dagger\left[1-\frac{a_i^\dagger a_i}{2S}\right]^{1/2};\ S_z^a(i)=S-a_i^\dagger a_i$$

on sublattice A, and by

$$S_+^b(i)=\sqrt{2S}\,b_i^\dagger\left[1-\frac{b_i^\dagger b_i}{2S}\right]^{1/2};\ S_-^a(i)=\sqrt{2S}\left[1-\frac{b_i^\dagger b_i}{2S}\right]^{1/2}b_i;\ S_z^b(i)=-S+b_i^\dagger b_i$$

on sublattice B. Introducing these representations into $H_{\rm AF}$ we obtain to first order in $1/S$, the following equivalent Hamiltonian for the antiferromagnet

$$H_S=-JZS^2+JZS\sum_{\mathbf{k}}[a_{\mathbf{k}}^\dagger a_{\mathbf{k}}+b_{\mathbf{k}}^\dagger b_{\mathbf{k}}+\gamma\mathbf{k}(a_{\mathbf{k}}^\dagger b_{\mathbf{k}}^\dagger+a_{\mathbf{k}}b_{\mathbf{k}})]\ , \quad (2.1)$$

where Z is the coordination number of the lattice, $a_{\mathbf{k}}^\dagger$ and $b_{\mathbf{k}}^\dagger$ are Fourier transforms of $a_i^\dagger$, and $b_i^\dagger$ and $\gamma_{\mathbf{k}}$ is defined by

$$\gamma\mathbf{k}=\frac{1}{Z}\sum_{\rm NN}e^{i\mathbf{k}\cdot\delta}\ . \quad (2.2)$$

The sum over δ extends over the nearest neighbors of any site of the lattice, and $\gamma\mathbf{k}$ is real on any lattice with inversion symmetry. It is easily shown that the ground state $|G\rangle$ of H_S is given by

$$|G\rangle=\exp\left[-\sum_{\mathbf{k}}\frac{\gamma\mathbf{k}}{(1-\gamma_{\mathbf{k}}^2+1)^{1/2}}a_{\mathbf{k}}^\dagger b_{\mathbf{k}}^\dagger\right]|0\rangle\ , \quad (2.3)$$

where $|0\rangle$ is the state with no bosons (the classical Néel state). Rewriting this state with real-space operators we obtain

$$|G\rangle=\exp\left[-\sum_{i\in A,j\in B}I(i-j)a_i^\dagger b_i^\dagger\right]|0\rangle\ , \quad (2.4)$$

where

$$I(\mathbf{r})=\frac{1}{v}\int_v\frac{d^dk}{(2\pi)^d}\frac{\gamma\mathbf{k}e^{i\mathbf{k}\cdot\mathbf{r}}}{(1-\gamma_{\mathbf{k}}^2+1)^{1/2}}\ , \quad (2.5)$$

v being the volume of the Brillouin zone. Undoing the Holstein Primakoff transformation, we see that to order $1/S$, the ground state of H is given by

$$|G\rangle=\exp\left[-\frac{1}{2S}\sum_{i\in A,j\in B}I(i-j)S_-^a(i)S_+^b(j)\right]|0\rangle\ . \quad (2.6)$$

An alternate approach is to treat the state in Eq. (2.6) as a variational ansatz for the ground state of the Heisenberg antiferromagnet. The constraint that no more than $2S$ bosons can occupy a given site, which is implicit in the Holstein-Primakoff transformation, will then have been taken into account exactly. The state in Eq. (2.6) is, however, complex enough to make calculation of the expectation value of $H_{\rm AF}$ quite difficult. An important simplification can, however, be made by noting the spatial dependence of $I(\mathbf{r})$. It can be shown from Eq. (2.5) that $I(\mathbf{r})\to|\mathbf{r}|^{-(d+1)}$ for large $|\mathbf{r}|$. We show in Table I the values of I for a few points for both the one-dimensional chain and two-dimensional square lattice. A notable feature of Table I is that the values of I are much larger for nearest neighbors than any other pair of sites: In 1D the nearest neighbor value of I is 59 times larger than any other bond, while in 2D the corresponding number is ten. We may therefore take as a reasonable variational wave function of the Heisenberg antiferromagnet the state

$$|\Psi\rangle=\exp\left[-\frac{1}{2S}\sum_{i\in A}\sum_{j\in i+\delta}gS_-^a(i)S_+^b(j)\right]\ . \quad (2.7)$$

We now treat g as a free variational parameter. From the spin-wave expansion we expect g to be nearly 0.36 in 1D and 0.16 in 2D. Specializing to the case of $S=\frac{1}{2}$ where $(\sigma_-^a)^2=0$, we obtain the variational wave function used in this paper in its final form:

$$|\Psi\rangle=\prod_{i\in A}\sum_{j\in i+\delta}[1-g\sigma_-^a(i)\sigma_+^b(j)]|0\rangle\ . \quad (2.8)$$

A. Exact results in one dimension

The expectation value of the state in Eq. (2.8) can be evaluated exactly in one dimension. This result depends upon the well-known Jordan-Wigner transformation[20] which establishes a connection between the Hilbert space of the Pauli matrices and that of a spinless fermion. The connection is established using the operator relationships

$$\sigma_+(i)=f_i^\dagger\exp\left[i\pi\sum_{j<i}f_j^\dagger f_j\right];\ \sigma_z(i)=2f_i^\dagger f_i-1\ , \quad (2.9)$$

where f_i is operator annhilating a Jordan-Wigner at the site i. Substituting Eq. (2.9) into Eq. (2.7), we obtain the following representation for the trial wave function:

$$|\Psi\rangle=\exp\left[-g\sum_n(f_{2n+1}^\dagger+f_{2n-1}^\dagger)f_{2n}\right]|0\rangle\ . \quad (2.10)$$

We have taken the A sublattice to be the even-numbered sites of the chain. It is now necessary to introduce the following Fourier transform representations of the Jordan-Wigner fermions

$$f_k^e=(2/N)^{1/2}\sum_n f_{2n}^\dagger e^{2ikn};\ f_k^0=(2/N)^{1/2}\sum_n f_{2n+1}e^{ik(2n+1)}\ , \quad (2.11)$$

TABLE I. Values of the function $I(\mathbf{r})$ in $d=1$ and $d=2$. The coordinates of $\mathbf{r}$ are represented by the integers in column 1 for $d=1$ and by the pairs of integers in column 3 for $d=2$.

	$d=1$		$d=2$
n	I	(n,m)	I
1	0.363	(1,0)	0.1579
3	0.0061	(1,2)	0.0155
5	0.0024	(0,3)	0.00834

where N is the number of sites in the chain. In terms of these operators, the state in Eq. (2.10) can be written in the following simple manner:

$$|\Psi\rangle = \prod_k (1-2g\cos k f_k^{0\dagger} f_k^{e\dagger})|0\rangle \ . \tag{2.12}$$

In a similar manner, the Hamiltonian H_{AF} can also be written in terms of the f_k^e and f_k^0 operators:

$$H_{AF} = J\sum_k [\cos k\,(f_k^e f_k^0 + f_k^{0\dagger} f_k^{e\dagger}) - f_k^e f_k^{e\dagger} - f_k^{0\dagger} f_k^0] + \frac{4}{N}\sum_{k_1 k_2 q} f_{k_1}^e f_{k_1+q}^{e\dagger} f_{k_2+q}^{0\dagger} f_{k_2}^0 \cos q \ . \tag{2.13}$$

The evaluation of the expectation value of the Hamiltonian in Eq. (2.13) in the state in Eq. (2.12) is now completely straightforward. We state the final result:

$$\frac{\langle H_{AF}\rangle}{NJ} = -\frac{1}{4} - \frac{(1-2g)}{2g(1+4g^2)^{1/2}}[(1+4g^2)^{1/2}-1] - \frac{1}{4g^2}[(1+4g^2)^{1/2}-1]^2 \ . \tag{2.14}$$

The energy is a minimum at $g=0.389$ where it takes a value of $-0.428J$ per bond. This is about 3% larger than the exact ground-state energy of $-0.443J$. It is also notable how close the value of g is to the spin-wave value of $g=0.36$. The magnitude of the sublattice magnetization $\langle \sigma_z(n)\rangle/2$ can also be calculated straightforwardly. We obtain

$$\langle \sigma_z(n)\rangle = (-1)^{2n}\left[\frac{2}{(1+4g^2)^{1/2}} - 1\right] , \tag{2.15}$$

which takes the value 0.289 at $g=0.389$. The classical value of this sublattice magnetization is 0.5 while the exact quantum value is 0.

B. Two dimensions

Exact evaluation of the expectation value of the state in Eq. (2.8) is not possible in two dimensions. However, we shall develop a renormalized perturbation series in g which leads to a very accurate estimate of the energy of the Heisenberg antiferromagnet in the state $|\Psi\rangle$. From the spin-wave estimates of the value of g of 0.16 in two dimensions, we anticipate that a naive expansion of the expectation value of the energy in g will not yield unreasonable results. A simple expansion of the expectation value of the energy in powers of g leads to the result

$$\frac{\langle\Psi|H_{AF}|\Psi\rangle}{\langle\Psi|\Psi\rangle} = \left[\frac{ZN}{2}\right] - [\tfrac{1}{4} - g + (Z-1)g^2 + \cdots] \ . \tag{2.16}$$

This has a minimum at $g_m = 1/(2Z-2)$ which is $\frac{1}{6}$ for the square lattice. Note that this value of g_m is very close to the spin-wave prediction of 0.16. The minimum energy is $-(1/3)J$ per bond. To make a more accurate estimate of the minimum energy and of g_m, one tedious but, in principle, straightforward method, is to obtain further terms in a naive expansion in powers of g. However, a little work shows that this procedure converges slowly and an improved procedure is necessary with a partial resummation of the power series in g. We will develop such a procedure in this section.

We begin by making a connection between the quantum mechanics of the state $|\Psi\rangle$ in Eq. (2.8) and the statistical mechanics of counting monomers, dimers, and loops on a square lattice—this statistical mechanical problem will in turn be shown to be related to a Grassmannian functional integral. The argument begins by noting that the state $|\psi\rangle$ consists of the sum of a large number of terms generated by expanding out the product of the factors $[1-g\sigma_-^a(i)\sigma_+^b(j)]$ on each bond. For any term in this expansion the contribution of every bond on the square lattice will either be the term 1 or the term $-g\sigma_-^a(i)\sigma_+^b(j)$. We graphically represent bonds which contribute the second term by placing a *dimer* on the bond. Two dimers cannot have a common site because

$$(\sigma_-^a)^2 = (\sigma_+^b)^2 = 0 \ .$$

We may therefore represent this state $|\Psi\rangle$ as follows:

$$|\Psi\rangle = \sum_{d\in\mathcal{D}} (-g)^{n(d)}|d\rangle \ , \tag{2.17}$$

where $\mathcal{D}$ is the set of all possible ways of putting an arbitrary number of dimers on a square lattice, and $n(d)$ is the number of dimers in the state d. The set $\mathcal{D}$ may also be described as the set of all monomer-dimer coverings of the square lattice by placing a monomer on all the empty sites. In the calculation of the expectation value of the energy, one complicating feature is that the overlap, $\langle d|d'\rangle$, between the two different dimer configurations $|d\rangle$ and $|d'\rangle$ is not zero. This feature is demonstrated by the example shown in Fig. 3. The two dimer configurations in Figs. 3(a) and 3(b) are not identical; nevertheless, the spin configurations they represent are identical because the set of sites which have a dimer on them is the same. Diagramatically, this may be seen in Fig.

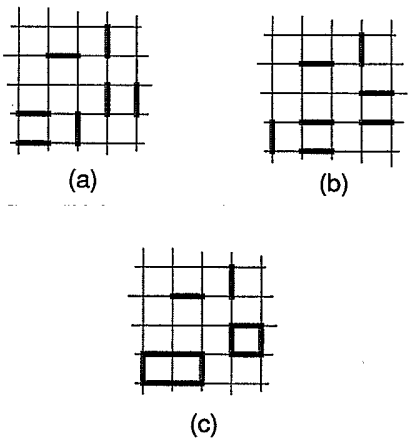

FIG. 3. Two terms, $|d>[(a)]$ and $|d'>[(b)]$, in the dimers expansion of $|\Psi\rangle$. The overlap $\langle d|d'\rangle$ is shown in (c).

3(c) where the two configurations have been overlaid. We see that while some dimers overlay exactly, the remaining form *closed loops*. It is now easy to see that the overlap $\langle\Psi|\Psi\rangle$ is given by

$$\langle\Psi|\Psi\rangle=\sum_{m\in\mathcal{M}}(g^2)^{n_d(m)}\prod(2g^l)^{n_l(m)}\,, \tag{2.18}$$

where $\mathcal{M}$ is the set of all possible monomer, dimer and loop coverings of the square lattice, $n_d(m)$ is the number of dimers in m, and $n_l(m)$ is the number of loops of size l in m. The loops yield an extra factor of 2 because there are two ways to obtain a loop from the overlap of two monomer-dimer coverings.

An efficient way of calculating the normalization and energy expectation value of $|\Psi\rangle$ is to map the problem of counting monomer-dimer-loop coverings of a square lattice onto a functional integral over Grassmannian fields. The procedure for carrying this out for a subset of the terms in Eq. (2.18) has already been developed by Samuel.[21] Samuel considered only monomer-dimer coverings, i.e., he evaluated the sum in Eq. (2.18) over all terms with $n_l(m)=0$ for all l. He showed in particular that this sum equals

$$\int\prod_i d\eta^\dagger(i)d\eta(i)\exp\left[\sum_i\eta^\dagger(i)\eta(i)+g^2\sum_{i\in A}\sum_{j\in i+\delta}\eta^\dagger(i)\eta(i)\eta^\dagger(j)\eta(j)\right],$$

where $\eta^\dagger(i)$ and $\eta(i)$ are Grassmannian variables at the site i. The validity of this result is easily seen by expanding the exponential and using $\eta^2=0$, $(\eta^\dagger)^2=0$, and the usual properties of Grassmannian integration $\int d\eta^\dagger d\eta=0$, $\int d\eta^\dagger d\eta\eta^\dagger=0$, and $\int d\eta^\dagger d\eta\eta^\dagger\eta=1$. We then see that the only nonzero terms in the expansion are those in which every site has a contribution from either the first term in the argument of the exponential (these are the sites with a monomer on them) or from the second term (these are the sites with a dimer on them). The properties of Grassmann numbers automatically take the hard core repulsion between the dimers into account.

The extension of Samuel's results to the case of interest in this paper is relatively straightforward. We simply add an additional interaction term in the functional integral for every different type of loop on the square lattice. A loop with l bonds will carry a prefactor $2g^l$; as g is small, this implies that the calculation can be carried out to a high degree of accuracy with only a small number of additional interaction terms. To order g^4, the only loop that needs to be considered is the elementary square plaquette. We therefore have the result

$$\langle\Psi|\Psi\rangle=\int\prod_i d\eta^\dagger(i)d\eta(i)e^S\,,$$

with

$$S=\sum_i\eta^\dagger(i)\eta(i)+g^2\sum_{i\in A}\sum_{j\in i+\delta}\eta^\dagger(i)\eta(i)\eta^\dagger(j)\eta(j)+2g^4\sum_{h,i,j,k\in\square}\eta^\dagger(h)\eta(h)\eta^\dagger(i)\eta(i)\eta^\dagger(j)\eta(j)\eta^\dagger(k)\eta(k)+\cdots\mathcal{O}(g^6)\,, \tag{2.19}$$

where in the third term the $\square$ indicates that the sum extends over all different sets of four numbers h,i,j,k which form an elementary plaquette. We will present results in this section to order g^4; the terms to order g^6 have also been calculated and will be discussed in Appendix A.

A particular advantage of the Grassmann functional integral representation is that properties of the antiferromagnet, like the sublattice magnetization and the ground-state energy, can be represented as local correlation functions of the Grassmann variables. The normalization of $|\Psi\rangle$ is taken into account by omitting the disconnected diagrams. We illustrate this procedure by considering the calculation of the sublattice magnetization M,

$$M=\frac{\langle\Psi|\sigma_z^a(i)|\Psi\rangle}{\langle\Psi|\Psi\rangle}\,. \tag{2.20}$$

In the expansion of $|\Psi\rangle$ in Eq. (2.17), every configuration d which has a dimer on site i will yield a factor of -1, while the remaining will yield a factor of $+1$. Now performing the expansion of both $|\Psi\rangle$ and $\langle\Psi|$ in M, we obtain

$$M=E_1-4(g^2E_2)-4(2g^4E_{4a})+\cdots\mathcal{O}(g^6)\,, \tag{2.21}$$

where we have introduced the quantities

$$\begin{aligned}E_1&=\text{Probability that site } i \text{ is empty in } \mathcal{M}\\&=\langle\eta^\dagger(i)\eta(i)\rangle\\&=\frac{\int\prod_j d_\eta^\dagger(j)d\eta(j)\eta^\dagger(i)\eta(i)e^S}{\int\prod_j d\eta^\dagger(j)d\eta(j)e^S}\,,\end{aligned} \tag{2.22}$$

g^2E_2 = Probability that site i is on a dimer in $\mathcal{M}$

$$=g^2\langle\eta^\dagger(i)\eta(i)\eta^\dagger(j)\eta(j)\rangle,\quad i,j \text{ nearest neighbors}, \tag{2.23}$$

$2g^4E_{4a}$ = Probability that site i is on a square loop in $\mathcal{M}$

$$=2g^4\langle\eta^\dagger(h)\eta(h)\eta^\dagger(i)\eta(i)\eta^\dagger(j)\eta(j)\eta^\dagger(k)\eta(k)\rangle,\quad h,i,j \text{ and } k \text{ on a square plaquette}. \tag{2.24}$$

The correlation functions E_1, E_2, and E_{4a} are represented graphically in Fig. 4—a shaded square is placed at every site which appears in the argument of the correlation function; the squares are connected by lines to show the relative position of the sites on the square lattice. The correlation functions can be evaluated in a renormalized power series expansion in g in a procedure very similar to that used by Samuel.[21] We introduce the Green's function

$$G\delta_{ij}=\langle\eta^\dagger(i)\eta(j)\rangle\ . \tag{2.25}$$

The bare value of this Green's function G^0 is 1. The full Green's function is determined in a *self-consistent* Hartree-Fock expansion in powers of g. As noted by Samuel, the use of this renormalized Green's function removes the slow convergence of the perturbation expansion of the correlation functions. Further details on the calculation of the Green's function and the correlation functions E_1, E_2, and E_{4a} are presented in Appendix A.

A very similar representation can also be obtained for the ground-state energy. We find

$$\frac{\langle\Psi|S_z(i)S_z(i+1)|\Psi\rangle}{\langle\Psi|\Psi\rangle}=-\tfrac{1}{4}E_2+\frac{g^2}{4}(4E_{3a}+2E_{3b}-E_2)-\frac{g^4}{4}(6E_{4a}+2E_{4b}+4E_{4c}+E_{4d})+\mathcal{O}(g^6)\ . \tag{2.26}$$

We have introduced five new correlation functions which are described by their diagrammatic representation in Fig. 4. Similarly,

$$\frac{\langle\Psi|S_x(i)S_x(i+1)+S_y(i)S_y(i+1)|\Psi\rangle}{\langle\Psi|\Psi\rangle}=-gE_2-2g^3E_{4a}+\mathcal{O}(g^5)\ . \tag{2.27}$$

Using the results of Appendix A we now have sufficient information to evaluate the ground-state energy, the sublattice magnetization, and the value of g_m. The results of this calculation are summarized in Table II. The small difference between the results of order g^4 and g^6 supports the contention that the perturbation expansion is very accurate. The best result at order g^6 yields a variational estimate for the ground-state energy of H_{AF} of $(-0.3317\pm0.0002)J$ per bond, occurring at a value of $g=g_m=0.1878$. As was the case in one dimension, the spin-wave estimate of $g_m=0.16$ was quite accurate. Our value of the ground-state energy is the lowest upper bound among existing variational calculations with a *single* variational parameter.[5,11] Our estimate of the sublattice magnetization (76% of the classical value) is somewhat higher than the estimates of Huse and Elser[5] (63%) and Reger and Young[6] (60%).

III. ANTIFERROMAGNET WITH ONE HOLE

We will now generalize the techniques introduced in the previous sections to obtain simple variational wave functions for the hole moving in a quantum Néel state. We present two closely related trial wave functions. The first wave function is presented in Sec. III A: its chief virtue is its simplicity; it is a useful trial wave function

TABLE II. Ground-state energy per bond, $E/2N$, and sublattice magnetization, M, of the Heisenberg antiferromagnet on a square lattice with exchange constant J. The results are presented to different orders in the variational parameter g.

Order	g	$E/(2NJ)$	M
2	0.15868	−0.32499	0.41468
4	0.18402	−0.33126	0.38478
6	0.18777	−0.33172	0.38008

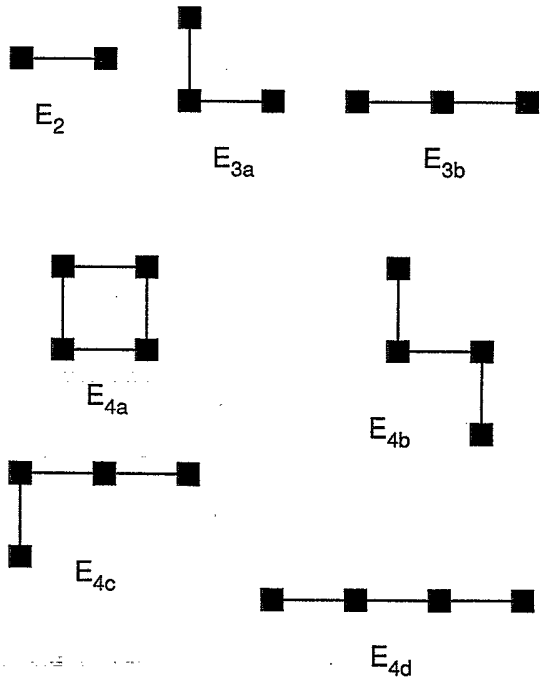

FIG. 4. Graphical representation of correlation functions of the functional integral in Eq. (2.19). Each figure represents a different correlation function given by a product of factors $\eta^\dagger(i)\eta(i)$ for each solid square. The lines have been drawn in to indicate the relative position of the sites on the square lattice.

only in the regime $J > 10t$. We nevertheless present a complete discussion of this simple wave function to clarify the concepts that will be needed for the second wave function. The weaknesses of this first wave function also help motivate the improved, but more complex wave function discussed in Sec. III B. The second wave function gives reliable estimates of the energy in the expanded regime $J > 0.25t$. The quantum Néel states considered will be very similar to those of the previous section: they will involve fluctuations of near-neighbor pairs of spins from the classical Néel state. The guiding principle of the calculation will be to include correctly all such near-neighbor spins flips correctly—all effects arising from the existence of long-range "dimers" will be ignored. The expansion parameter which makes this a reasonable working hypothesis is $1/(2Z-2)$.

A. Wave function I

We begin the discussion by considering a classical Néel state with spins up on sublattice A and down on sublattice B. Create a hole by removing an up-spin electron from the A sublattice site $\mathbf{r}_a$; this state will be denoted by the ket $|\mathbf{r}_a^0\rangle$. This state is represented pictorially in Fig. 5(a)—the solid circle represents the position of the hole. We may now include the quantum fluctuation of the background antiferromagnet by flipping pairs of spins on all bonds of $|\mathbf{r}_a^0\rangle$ except those adjacent to the hole; this is represented pictorially in Fig. 5(a) by omitting the lines through the bonds which cannot have a dimer placed on them. This renormalized state will be labeled $|\mathbf{r}_a\rangle$,

$$|\mathbf{r}_a\rangle = \frac{1}{K_a} \prod_{i,j\mathrm{NN}}{}' [1 - g_a(i,j)\sigma_-^a(i)\sigma_+^b(j)]|\mathbf{r}_a^0\rangle \ , \quad (3.1)$$

where K_a is a normalization factor which insures $\langle \mathbf{R}_a|\mathbf{r}_a\rangle = 1$, and the prime on the product indicates that it only extends over all sites except those with no line through them in Fig. 5(a). Notice that the variational parameters $g_a(i,j)$ now depend upon the *relative* position of the bond from the hole. This wave function can be qualitatively interpreted as a polaronlike state with the size of the polaron being the distance over which the $g(i,j)$ vary from the location of the hole. We have organized the states so that the hole is at the center of the polaron. This is not an intrinsic limitation; any polaron wave function can be rearranged so as to make this the case.

Now consider moving the hole in $|\mathbf{r}_a^0\rangle$ to the B sublattice. Since the electrons conserve their spin while hopping, we will always obtain *one* spin with no accompanying partner, which has been flipped with respect to the classical Néel state. The four states which can be obtained by a single hop from $|\mathbf{r}_a^0\rangle$ are labeled $|\mathbf{r}_b^0;\alpha\rangle(\alpha=1,2,3,4)$; one of them ($\alpha=1$) is shown in Fig. 5(b), and the $\alpha=2,3,4$ states are 90, 180, and 270° rotations of the $\alpha=1$ state. The diamond in the figure denotes the position of the single flipped spin. Quantum fluctuations of the antiferromagnet can now be included as before: we flip pairs of spins on all bonds except those with no line through them in Fig. 5(b). We therefore obtain the states $|\mathbf{r}_b;\alpha\rangle$,

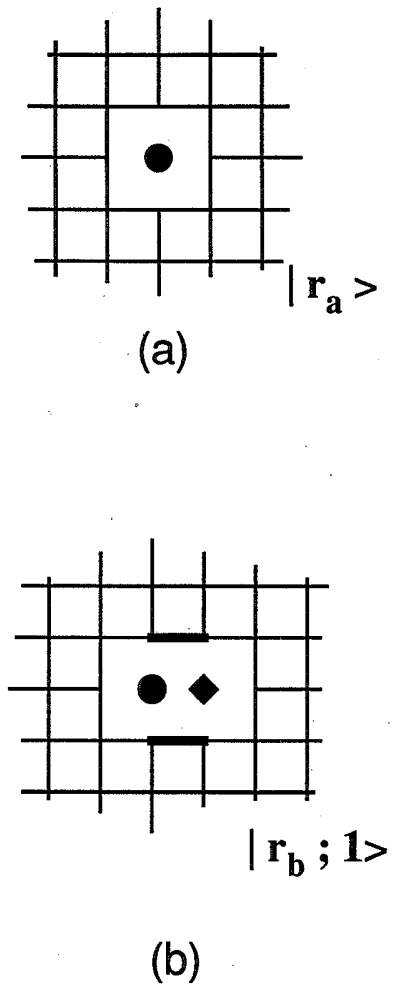

FIG. 5. Graphical representation of the states $|\mathbf{r}_a\rangle$ and $|\mathbf{r}_b;1\rangle$. The states $|\mathbf{r}_b;2$ to $4\rangle$ are rotations of $|\mathbf{r}_b;1\rangle$. The solid circle represents the position of the hole and the diamond represents a single spin-flip from the background Néel state. Dimer spin-pair fluctuation can occur on all sites except those, adjacent to the hole and the single spin flip, which do not have a line drawn through them. The darkened bonds in (b) indicate the locations where the $g_{b1}(i,j)$ values become large in the energy minimization.

$$|\mathbf{r}_b;\alpha\rangle = \frac{1}{K_{b\alpha}} \prod_{i,j\mathrm{NN}}{}' [1 - g_{b\alpha}(i,j)\sigma_-^a(i)\sigma_+^b(j)]|\mathbf{r}_b^0;\alpha\rangle \ , \quad (3.2)$$

where again the prime denotes that the product extends over all but the empty bonds of Fig. 5(b).

Further motion of the hole from $|\mathbf{r}_b;\alpha\rangle$ will either take the system to a state with nonzero overlap with $|\mathbf{r}_a\rangle$, or to a state with the hole on sublattice A but with a non-near-neighbor pair of spins flipped. As discussed earlier, such states do not appear to leading order in $1/(2Z-2)$ in the antiferromagnet, and will be ignored. Therefore no further states need be considered. The problem has therefore been reduced to the diagonalization of a $5N/2 \times 5N/2$ matrix which is a function of the infinite

number of parameters $g_a(i,j)$ and $g_{b\alpha}(i,j)$. Translational invariance and Fourier transformation reduce the matrix to a 5×5 matrix which can easily be diagonalized.

As was apparent in the previous sections, the states in Eqs. (3.1) and (3.2) are still too complicated for an exact evaluation of the matrix elements of the Hamiltonian. However, if $|g_a(i,j)|$ and $|g_{b\alpha}(i,j)|$ are small, then an approximate evaluation of the matrix elements in powers of the g parameters is possible. The procedure we shall follow can therefore be outlined as follows:

(i) The matrix elements of H_h are evaluated to second order in g. The mechanics of the evaluation of the matrix elements is discussed in Appendix B.

(ii) The 5×5 matrix so obtained is diagonalized and its lowest eigenvalue determined as a function of the wavevector $\mathbf{k}$ and the parameters $g_a(i,j)$ and $g_{b\alpha}(i,j)$

(iii) The values of $g_a(i,j)$ and $g_{b\alpha}(i,j)$ which minimize the lowest eigenvalue are determined for each $\mathbf{k}$.

(iv) For consistency, it is now required that the values of the g parameters at the minimum be small enough to justify the approximations made in the evaluation of the matrix elements.

An important feature of the calculation becomes apparent when this procedure is followed. It is found that even for small values of J/t, the values of $g_a(i,j)$ and $g_{b\alpha}(i,j)$ at a bond which minimize the energy are determined to a good approximation by the coordination number of the bond. Two consequences of this fact are as follows: (i) The values of the parameters $g_a(i,j)$ and $g_{b\alpha}(i,j)$ return to their values in the hole-free antiferromagnet $[1/(2Z-2)]$ within three to four lattice spacings of the hole. This fact can be used to reduce the computer time necessary in determining the minimum of the lowest eigenvalue. (ii) The bonds which are most likely to violate the consistency requirement in step (iv) above are those with the weakest coordination. This is indeed what happens. It is found that the values of the g parameters on the bonds which are drawn with a thick line in Fig. 5(b) become unacceptably large for $J/t<10$; these are the bonds with the smallest coordination. A heartening feature of the calculation is, however, that on *all* other bonds the g parameters remain smaller than 0.4 all the way down to $J/t=0.3$.

The chief insight gained from the calculation above is that, to obtain reliable values of the hole energy for smaller values of J/t, it will be necessary to treat exactly the spins on the darkened bonds in Fig. 5(b) by expanding the set of basis states with hole on sublattice B; no changes will be necessary for the states with the hole on sublattice A because none of the $g_a(i,j)$ parameters became large even for small values of J/t. The procedure for carrying this out will be discussed in the next section.

B. Wave function II

The spins on the darkened bonds in Fig. 5(b) can be treated exactly by expanding the basis states $|\mathbf{r}_a^0\rangle$ and $|\mathbf{r}_b^0;\alpha\rangle$ upon which the dimers are placed. The new basis states will be labeled $|\mathbf{R}_a^0\rangle$ and $|\mathbf{R}_b^0;\alpha\rangle(\alpha=1$ to 12) and are shown in Fig. 6. There are a total of 13 basis states and the dimers are placed upon all but the empty bonds

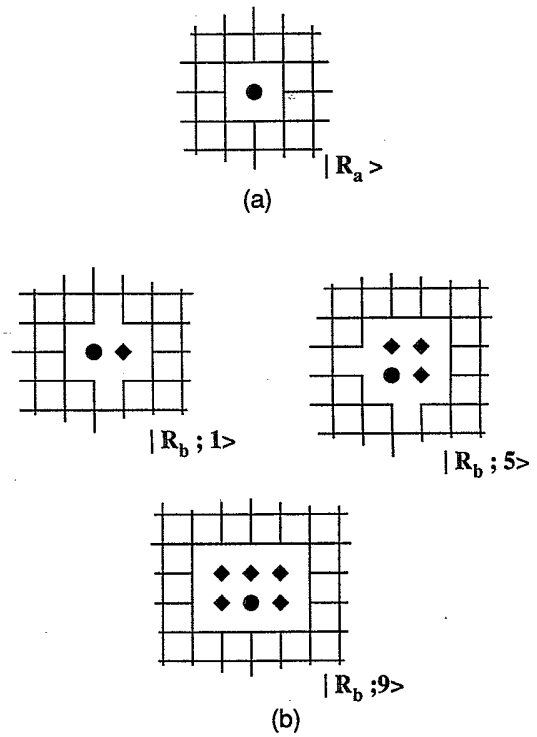

FIG. 6. Graphical representation of the states $|\mathbf{R}_a\rangle$, $|\mathbf{R}_b;1\rangle$, $|\mathbf{R}_b;5\rangle$, and $|\mathbf{R}_b;9\rangle$. The states $|\mathbf{R}_b;2$ to $4\rangle$, $|\mathbf{R}_b;6$ to $8\rangle$, and $|\mathbf{R}_b;10$ to $12\rangle$ are rotations of $|\mathbf{R}_b;1\rangle$, $|\mathbf{R}_b;5\rangle$, and $|\mathbf{R}_b;9\rangle$, respectively. The solid circle represents the position of the hole and the diamonds represent a single spin-flip from the background Néel state. Dimer spin-pair fluctuations can occur on all sites except those, adjacent to the hole and the diamonds, which do not have a line drawn through them.

in Fig. 6. Notice that the spins on the sites with the darkened bonds in Fig. 5(b) have now been fixed. The full trial states $|\mathbf{R}_a\rangle$ and $|\mathbf{R}_b;\alpha\rangle$ are obtained as before:

$$|\mathbf{R}_a\rangle=\frac{1}{K_a}\prod_{i,j\mathrm{NN}}{}'\,[1-G_a(i,j)\sigma_-^a(i)\sigma_+^b(j)]|\mathbf{R}_a^0\rangle\ , \tag{3.3}$$

$$|\mathbf{R}_b;\alpha\rangle=\frac{1}{K_{b\alpha}}\prod_{i,j\mathrm{NN}}{}'\,[1-G_{b\alpha}(i,j)\sigma_-^a(i)\sigma_+^b(j)]|\mathbf{R}_b^0;\alpha\rangle\ , \tag{3.4}$$

where again the primes indicate that the product extends over all but the empty bonds in Fig. 6, and a new set of variational parameters $G_a(i,j)$ and $G_{b\alpha}(i,j)$ have been introduced. The remaining procedure exactly parallels that described in Sec. III A: the matrix elements of H_h are evaluated to second order in the $G(i,j)$'s, the resulting 13×13 matrix is diagonalized, and its lowest eigenvalue is minimized as a function of the $G(i,j)$'s. The subsequent discussion is divided into two sections: Sec. III B 1 presents the results of the calculation and Sec. III B 2 discusses the possible sources of error in the results. Questions on the convergence of the calculation are also discussed.

1. Results

The results of the calculation are presented in Figs. 1, 2, and 7. Figure 1 shows the energy of the hole E/t at the three different momenta (0,0), $(\pi,0)$ and $(\pi/2,\pi 2)$ as a function of J/t. The zero of energy is the energy of the antiferromagnet with one hole and $t=0$. For all values of J/t the global minimum state is always at the momentum $(\pi/2,\pi/2)$. We show in Fig. 2(a) the bandwidth of the hole

$$W/t=E/t(\mathbf{k}=(0,0))-E/t(\mathbf{k}=(\pi/2,\pi/2)) .$$

Note the maximum in the bandwidth at $J=0.73t$ where $W=1.24t$. At large values of J/t we find $W\approx 2.6t^2/J$; the proportionality of the bandwidth on t^2/J can be seen from a large J/t perturbation theory for the hole, although calculation of the coefficient requires the nontrivial calculations of this paper. For small J/t, Fig. 2(b) indicates that $W\approx 3.4J$. It is clearly of interest to find other methods of calculating the hole bandwidth to see if this behavior persists into the regime $J/t<0.25$. Some of the points in Fig. 1 have been tabulated for reference in Table III. Figure 7 displays the energy-momentum relationship of the hole on a line from the zone center to the zone-boundary point $(\pi,0)$ for the case $J/t=2.0$.

2. Error estimation

The uncertainties in the results of Sec. III B 1 arise from three different sources.

(i) Truncation of the infinite set of variational parameters. The variational parameters $G_a(i,j)$ and $G_{ba}(i,j)$ must necessarily be truncated to some finite set which is allowed to vary freely, while the remaining are fixed at their values in the hole-free antiferromagnet. However, as noted in Sec. III A, the dimer nature of wave function makes the value of any $G_a(i,j)$ or $G_b(i,j)$, which is greater than four lattice spacings from the hole, essentially equal to that of the hole-free antiferromagnet. Calculations were performed with as many as 236 different variational parameters, although it was found that reasonable results were obtained over the entire range of J/t values considered with as few as 68 variational parameters. We estimate the error in the results from this source to be smaller than $0.01t$ for all J/t.

(ii) Approximate evaluation of the matrix elements of H_h. All the matrix elements of the Hamiltonian are evaluated to second order in $G(i,j)$. The values of $|G(i,j)$ are all less than $G_{\max}=0.3$ for $J/t>1$ but a *few* (~ 10) of them start to become larger as J/t decreases. For $J/t>0.6$, $G_{\max}$ equals 0.4, while $G_{\max}$ equals 0.5 for $J/t>0.25$. Each individual matrix element of the Hamiltonian is actually a power series in $G(i,j)^2$, so the relative error in each matrix element and in the bandwidth of order $G_{\max}^2$. Therefore the uncertainty in the bandwidth, $\Delta W/W$, satisfies $\Delta W/W<9\%$ for $J/t>1.0$, $\Delta W/W<16\%$ for $J/t>0.6$, and $\Delta W/W<25\%$ for $J/t>0.25$. We emphasize however that these are very conservative upper bounds on the error: the large majority of the $G(i,j)$ values are considerably smaller than 0.3 for all J/t. Since the matrix elements of the Hamiltonian always involve products of the $G(i,j)$ on neighboring bonds, the relative error in the matrix elements is probably much smaller than we have estimated earlier. Also, the simple second-order approximation for the antiferromagnet gives much better results than would be expected from an error estimate similar to the one above.

(iii) Inadequacy of the dimer form of the wave function. The relative errors from this source are the hardest to estimate. However, the fact that the $G(i,j)$ parameters are small is itself an indication of the adequacy of the trial wave function. If true wave function was locally completely different from the background Néel state, we expect that the variational calculation would signal this by making the $G(i,j)$ parameters comparable to unity. This is precisely what happened with the wave function in Sec. III A: the values of the $g(i,j)$ grew large on a particular set of bonds indicating that spin correlations on those sites were poorly described by the dimer approximation. The improved calculation in this section treated exactly the relative spin configurations on these bonds. No analogous signal appeared in the calculation with wave function II, indicating that all the remaining bonds are satisfactorily described by the dimer approximation.

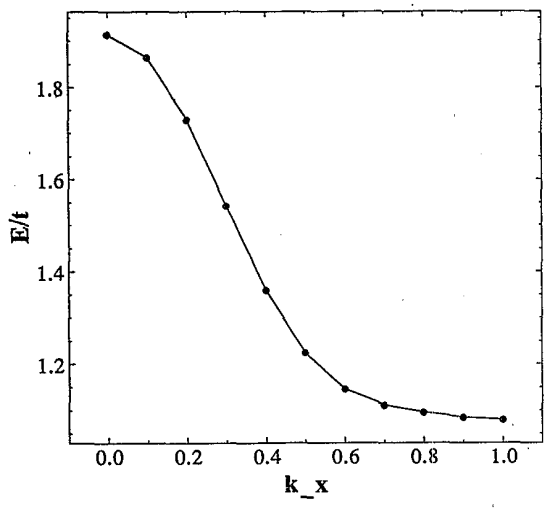

FIG. 7. Energy-momentum relationship of the hole on a line from the zone center to the zone-boundary point $(\pi,0)$ at a value of $J/t=2.0$; the momentum is $\pi(k\_x,0)$.

TABLE III. Energy of a single hole in units of the hopping parameter t for different exchange constants J and momenta $\mathbf{k}$. The zero of energy is the ground-state energy of the antiferromagnet with *one hole* and $t=0$.

J/t	$\mathbf{k}=(0,0)$	$\mathbf{k}=(\pi,0)$	$\mathbf{k}=(\pi/2,\pi/2)$
10	−0.069	−0.28	−0.33
6	−0.12	−0.46	−0.54
2	−0.34	−1.15	−1.28
1	−0.64	−1.71	−1.84
0.6	−1.01	−2.10	−2.24
0.3	−1.78	−2.56	−2.76
0.25	−2.03	−2.67	−2.91

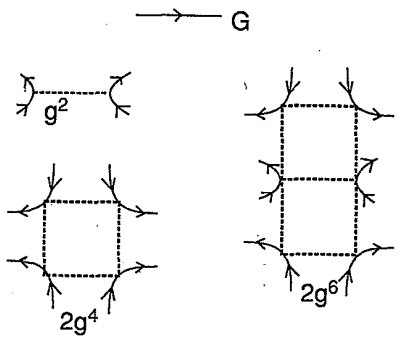

FIG. 8. Green's function G and the three interaction vertices of the action S_6. The dashed lines indicate the relative position of the fermions involved in the interaction.

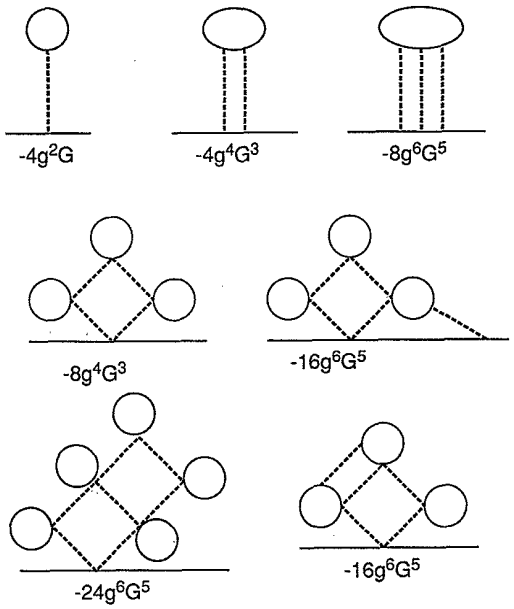

FIG. 9. Graphs for the self-energy Σ to order g^6. The values of the graphs include all the symmetry factors and the different possible orientations of the interaction vertices.

IV. CONCLUSIONS

This paper has presented a reasonable variational basis for determining the energy-momentum relation of a single hole moving in a background Néel state. The Néel state is described as a classical Néel state superposed by a dilute uncorrelated gas of near-neighbor spin flips (dimers). The small parameter which makes the density of dimers small is the inverse of the coordination number $[=1/(2Z-2)=\frac{1}{6}]$ of a bond on the square lattice. The minimum hole energy occurs at the zone boundary point $\mathbf{k}=(\pi/2,\pi/2)$. The bandwidth W is a nonmonotonic function of J/t and achieves a maximum value at $J/t=0.73$. It obeys $W\approx 2.6t^2/J$ for large J/t and appears to decrease linearly with J ($W\approx 3.4J$) for small J/t. The decrease in the bandwidth W is consistent with the enhancement of the hole mass observed in optical absorption experiments.[18]

An intermediate result of our calculation was the determination of a variational upper bound of $(-0.3317\pm 0.0002)J$ on the ground-state energy per bond of the square lattice spin-$\frac{1}{2}$ antiferromagnet. This compares favorably with estimate of the ground-state energy $(-0.334\pm 0.001)J$ made by Huse using series expansions.[10] It is also the lowest upper bound among existing variational calculations with a *single* variational parameter.[5,11]

Several other problems can be attacked using the approach of this paper. The simplest is probably the determination of the $S=1$ excitation spectrum of the antiferromagnet. This will lead to a value for the renormalized spin-wave velocity. A more difficult problem is the determination of the two and multimagnon excitation spectrum; the solution of this problem could possibly shed some light upon the light scattering experiments of Lyons *et al.*[22]

It would also be of interest to determine changes in the configuration of the spins in the neighborhood of a single hole in an antiferromagnet as a function of t/J. This information is, in principle, contained in the eigenvectors of the 13×13 matrix diagonalized in Sec. III B and the values of the $G(i,j)$ parameters at the minimum energy. The analysis of these results is, however, complicated by the fact that the hole eigenstates are Bloch wavelike states, whereas the results are best understood in a local Wannier representation. The analysis is deferred to a future publication.

ACKNOWLEDGMENTS

I would like to acknowledge useful discussions with D. A. Huse, N. Read, R. Shankar, B. I. Shraiman, and C. M. Varma. L. Krauss provided valuable assistance in generating the figures. I thank C. Henley for pointing out an error in a previous version of the paper.

APPENDIX A

In this appendix we present details of the calculation of the expectation values of the energy and the sublattice magnetization using the functional integral method. Terms up to order g^6 will be included. The action of the functional integral was presented correct to order $g^4(S_4)$ in Eq. (2.19); there is only one additional term in the action at order g^6 corresponding to the single six-sided loop (covering two adjacent plaquettes) that can be drawn on the square lattice (this loop will be represented by the symbol ⊡).

$$S_6=S_4+\sum_{abcdef\in\boxdot}\eta^\dagger(a)\eta(a)\eta^\dagger(b)\eta(b)\eta^\dagger(c)\eta(c)\eta^\dagger(d)\eta(d)\eta^\dagger(e)\eta(e)\eta^\dagger(f)\eta(f)\ . \tag{A1}$$

We now present details of the diagrammatic evaluation of the correlation functions. The renormalized Green's func-

tion G will be represented by a full line as shown in Fig. 8. Also shown in Fig. 8 are the three interaction vertices present at order g^6. The Green's function G can be represented in the form

$$G=\frac{1}{1-\Sigma}\ , \tag{A2}$$

where the self-energy Σ is the sum of all the one-particle irreducible graphs. All the terms in Σ to order g^6 are shown in Fig. 9. This yields the expression

$$\Sigma=-4g^2G-12g^4G^3-64g^6G^5\ . \tag{A3}$$

Solution of Eqs. A2 and A3 yields the value of the renormalized Green's function.

The ground-state energy to $\mathcal{O}(g^6)$ involves the following expectation values:

$$\frac{\langle\Psi|S_z(i)S_z(i+1)|\Psi\rangle}{\langle\Psi|\Psi\rangle}=-\tfrac{1}{4}E_2+\frac{g^2}{4}(4E_{3a}+2E_{3b}-E_2)$$
$$-\frac{g^4}{4}(6E_{4a}+2E_{4b}+4E_{4c}+E_{4d})-\frac{g^6}{4}(22E_{6a}+8E_{6b}+8E_{6b}+8E_{6c})-\mathcal{O}(g^8)\ , \tag{A4}$$

where we have introduced the three new correlation functions E_{6a}, E_{6b}, and E_{6c}; these functions are defined by the diagrammatic representations in Fig. 10. Similarly,

$$\frac{\langle\Psi|S_x(i)S_x(i+1)+S_y(i)S_y(i+1)|\Psi\rangle}{\langle\Psi|\Psi\rangle}=-gE_2-2g^3E_{4a}-6g^5E_{6a}-\mathcal{O}(g^7)\ . \tag{A5}$$

Finally we quote to order g^6 the expression for the sublattice magnetization M,

$$M=E_1-4(g^2E_2)-4(2g^4E_{4a})-12(2g^6E_6)-\cdots\mathcal{O}(g^8)\ . \tag{A6}$$

It is now necessary to calculate the various E_i correlation functions using the Grassmann functional integral. The first step involves the reduction of these correlation functions into their various disconnected pieces. For example, the correlation function E_2 has the decomposition

$$E_2=\langle\eta^\dagger(i)\eta(i)\eta^\dagger(j)\eta(j)\rangle$$
$$=\langle\eta^\dagger(i)\eta(i)\rangle\langle\eta^\dagger(j)\eta(j)\rangle+\langle\eta^\dagger(i)\eta(i)\eta^\dagger(j)\eta(j)\rangle_C\ , \tag{A7}$$

where the C subscript on the second correlation function indicates that it involves only connected correlation functions. We denote this connected correlation function by the symbol C_{2a}, and represent it graphically in Fig. 11(a): as with the E correlation functions, the solid squares represent the various points in the arguments of the correlation functions, and the dark lines are drawn in to represent the relative location of the points on the lattice. The equation A7 may therefore be rewritten,

$$E_2=G^2+C_{2a}\ . \tag{A8}$$

Similar decomposition of the remaining E correlation functions can also be made. We find it necessary to introduce 20 new connected correlation functions which are defined by their diagrammatic representations in Figs. 11(a) and 11(b). They are denoted by the symbols $C_{i\alpha}$ where the number i ($i\in1$ to 6) denotes a i-point connected correlation function and α is a label distinguishing the various i-point functions. The expressions for the E correlation functions can then be calculated to be as follows. The decomposition of the three-point functions are completely straightforward:

$$\begin{aligned}E_{3a}&=G^3+2C_{2a}G+C_{2b}G-C_{3a}\ ,\\ E_{3b}&=G^3+2C_{2a}G+C_{2c}G-C_{3b}\ .\end{aligned} \tag{A9}$$

The four-point functions are a little more complex:

$$\begin{aligned}E_{4a}&=G^4+4C_{2a}G^2+2C_{2b}G^2+2C_{2a}^2+C_{2b}^2-4C_{3a}G+C_{4a}\ ,\\ E_{4b}&=G^4+3C_{2a}G^2+2C_{2b}G^2+C_{2d}G^2+C_{2a}^2+C_{2b}^2+C_{2a}C_{2d}-2C_{3c}G-2C_{3a}G+C_{4b}\ ,\\ E_{4c}&=G^4+3C_{2a}G^2+2C_{2b}G^2+C_{2d}G^2+C_{2c}G^2+C_{2a}^2+C_{2a}C_{2d}+C_{2b}C_{2c}-C_{3a}G-C_{3b}G-C_{3c}G-2C_{3d}G+C_{4c}\ ,\\ E_{4d}&=G^4+3C_{2a}G^2+2C_{2c}G^2+C_{2e}G^2+C_{2a}^2+C_{2a}C_{2e}+C_{2c}^2-2C_{3b}G-2C_{3e}G+C_{4d}\ .\end{aligned} \tag{A10}$$

The decomposition of the six-point functions into connected correlation functions is, however, an order of magnitude more complex; we nevertheless display the results here for reference.

$$E_{6a}=G^6+7C_{2a}G^4+4C_{2b}G^4+2C_{2c}G^4+2C_{2d}G^4+11C_{2a}^2G^2+3C_{2a}^3+2C_{2a}^2C_{2d}+8C_{2a}C_{2b}G^2$$
$$+2C_{2a}C_{2b}^2+4C_{2a}C_{2b}C_{2c}+6C_{2a}c_{2c}G^2+C_{2a}C_{2c}^2+6C_{2a}C_{2d}G^2+C_{2a}C_{2d}^2+4C_{2b}^2G^2+2C_{2b}^2C_{2d}$$
$$+4C_{2b}C_{2c}G^2+4C_{2b}C_{2d}G^2+C_{2c}^2G^2+C_{2d}^2G^2-(8C_{3a}+2C_{3b}+4C_{3c}+4C_{3d}+2C_{3f})G^3$$
$$-[4C_{3a}(3C_{2a}+C_{2b}+C_{2c}+C_{2d})+2C_{3b}(2C_{2a}+C_{2c})+4C_{3c}(C_{2a}+C_{2b}+C_{2d})$$
$$+4C_{3d}(2C_{2a}+C_{2b})+2C_{3f}(2C_{2b}+C_{2c})]G+2C_{3a}^2+4C_{3a}C_{3d}+C_{3b}^2+2C_{3c}^2$$
$$+2C_{4a}G^2+2C_{4a}C_{2a}+2C_{4b}G^2+2C_{4b}C_{2d}+4C_{4c}G^2+4C_{4c}C_{2a}+2C_{4e}G^2+2C_{4e}C_{2c}$$
$$+4C_{4f}G^2+4C_{4f}C_{2b}+C_{4g}G^2+C_{4g}C_{2a}-C_{5a}G-C_{5b}G+C_6\ , \tag{A11}$$

$$E_{6b}=G^6+6C_{2a}G^4+3C_{2b}G^4+2C_{2c}G^4+2C_{2d}G^4+C_{2e}8C_{2a}^2G^2+2C_{2a}^3+C_{2a}^2C_{2d}+C_{2a}^2C_{2e}$$
$$+5C_{2a}C_{2b}G^2+C_{2a}C_{2b}^2+C_{2a}C_{2b}C_{2c}+4C_{2a}C_{2c}G^2+C_{2a}C_{2c}^2+5C_{2a}C_{2d}G^2+C_{2a}C_{2d}^2+C_{2a}C_{2d}C_{2e}$$
$$+3C_{2a}C_{2e}G^2+2C_{2b}^2G^2+C_{2b}^2C_{2e}+3C_{2b}C_{2c}G^2+2C_{2b}C_{2c}C_{2d}+2C_{2b}C_{2d}G^2+2C_{2b}C_{2e}G^2$$
$$+C_{2b}^2C_{2e}+C_{2c}^2G^2+2C_{2c}C_{2d}G^2+C_{2d}^2G^2+C_{2d}C_{2e}G^2-(5C_{3a}+2C_{3b}+3C_{3c}+2C_{3d}+2C_{3e}+C_{3f})G^3$$
$$-[C_{3a}(6C_{2a}+C_{2b}+2C_{2c}+2C_{2d}+2C_{2e})+C_{3b}(3C_{2a}+C_{2b}+C_{2d})+2C_{3d}(C_{2a}+C_{2c}+C_{2d})$$
$$+C_{3c}(3C_{2a}+2C_{2b}+C_{2c}+C_{2d}+2C_{2e})+C_{3e}(3C_{2a}+2C_{2b}+C_{2d})+C_{3f}(C_{2b}+C_{2c})]G$$
$$+C_{3a}C_{3c}+C_{3a}C_{3e}+C_{3a}C_{3b}+C_{3d}^2+C_{3d}C_{3e}+C_{4a}G^2+C_{4a}C_{2a}+C_{4b}G^2+2C_{4b}C_{2e}$$
$$+2C_{4c}G^2+C_{4c}C_{2a}+C_{4c}C_{2d}+C_{4d}G^2+C_{4d}C_{2a}+C_{4e}G^2+C_{4f}G^2+C_{4f}C_{2c}-C_{5a}G\ , \tag{A12}$$

$$E_{6c}=G^6+6C_{2a}G_4+4C_{2b}G^4+C_{2c}G^4+3C_{2d}G^4+8C_{2a}^2G^2+2C_{2a}^3+2C_{2a}^2C_{2d}+7C_{2a}C_{2b}G^2+2C_{2a}C_{2b}^2$$
$$+C_{2a}C_{2b}C_{2c}+2C_{2a}C_{2c}G^2+8C_{2a}C_{2d}G^2+2C_{2a}C_{2d}^2+4C_{2b}^2G^2+2C_{2b}^2C_{2d}+2C_{2b}C_{2c}G^2+C_{2b}C_{2c}C_{2d}$$
$$+5C_{2b}C_{2d}G^2+C_{2c}C_{2d}G^2+2C_{2d}^2G^2-(6C_{3a}+C_{3b}+5C_{3c}+2C_{3d}+C_{3f})G^3$$
$$-[C_{3a}(8C_{2a}+3C_{2b}+C_{2c}+4C_{2d})+C_{3b}(C_{2a}+C_{2d})+C_{3c}(5C_{2a}+4C_{2b}+C_{2c}+5C_{2d})$$
$$+C_{3d}(3C_{2a}+2C_{2b}+C_{2b}+C_{2d})+2C_{3f}C_{2b}]G+C_{3a}^2+C_{3a}C_{3c}+C_{3a}C_{3d}+C_{3c}^2$$
$$+C_{3c}C_{3d}+C_{4a}G^2+C_{4a}C_{2a}+2C_{4b}G^2+C_{4b}C_{2a}+C_{4b}C_{2d}+C_{4c}G^2+C_{4c}C_{2d}+C_{4e}G^2$$
$$+C_{4f}G^2+C_{4f}C_{2b}-C_{5a}G\ . \tag{A13}$$

The C correlation functions can be calculated according to the usual Feynman rules. We show in Fig. 12 the Feynman graph expansion for the correlation function C_{2a}. The results of such a calculation yield to order g^6 the following results for the two-point functions:

$$C_{2a}=g^2G^4+6g^4G^6+29g^6G^8\ ,$$
$$C_{2b}=-8g^6G^8,\quad C_{2c}=-g^4G^6-8g^6G^8\ , \tag{A14}$$
$$C_{2d}=g^6G^8,\quad C_{2e}=g^6G^8\ ,$$

three-point functions,

$$C_{3a}=-12g^6G^9,\quad C_{3b}=-2g^4G^7-16g^6G^9\ ,$$
$$C_{3c}=2g^6G^9,\quad C_{3d}=3g^6G^9\ , \tag{A15}$$
$$C_{3e}=2g^6G^9,\quad C_{3f}=0g^6G^9\ ,$$

four-point functions,

$$C_{4a}=2g^4G^8g^6G^{10},\quad C_{4b}=2g^6G^{10}\ ,$$
$$C_{4c}=4g^6G^{10},\quad C_{4d}=4g^6G^{10}\ ,$$
$$C_{4e}=4g^6G^{10},\quad C_{4f}=0g^6G^{10}\ , \tag{A16}$$
$$C_{4g}=2g^6G^{10}\ ,$$

five-point functions,

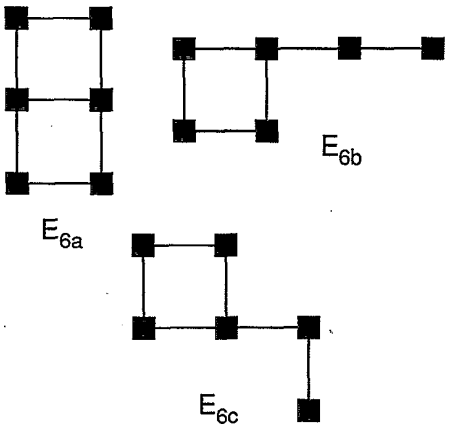

FIG. 10. Additional correlation functions of the type in Fig. 4 which appear at order g^6.

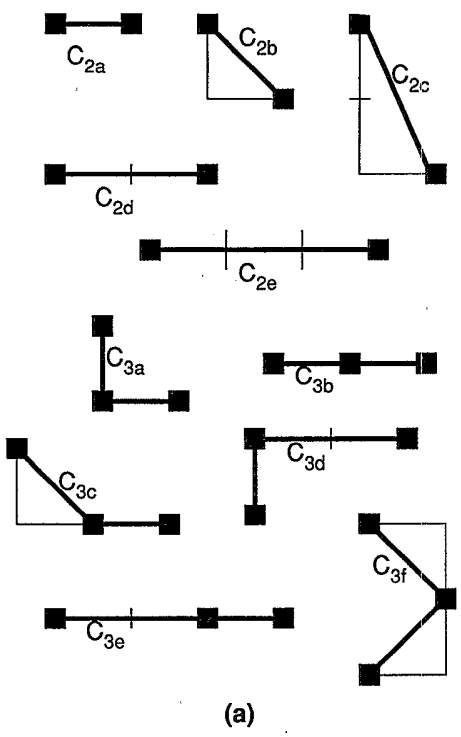

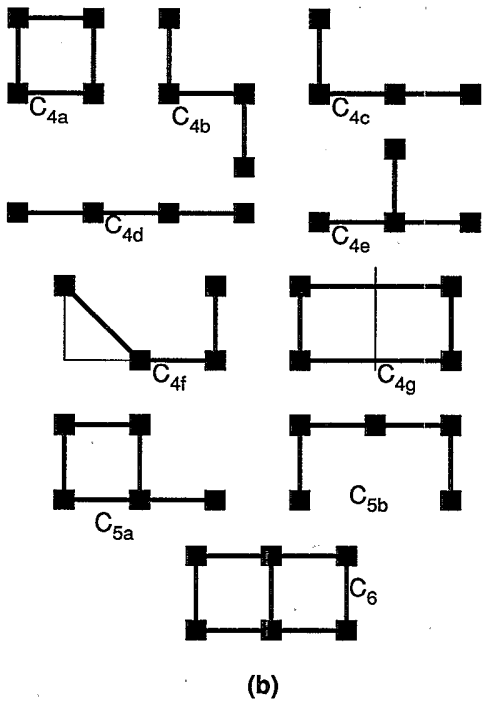

FIG. 11. Graphical representation of the *connected* correlation functions. The rules for the representation are identical to those of Fig. 4; the solid squares represent the sites which contribute a factor of $\eta^{\dagger}(i)\eta(i)$ to the correlation function and the lines indicate the relative position of the points on the square lattice. The lines have, however, been drawn in thicker to emphasize the connected nature of the correlation functions.

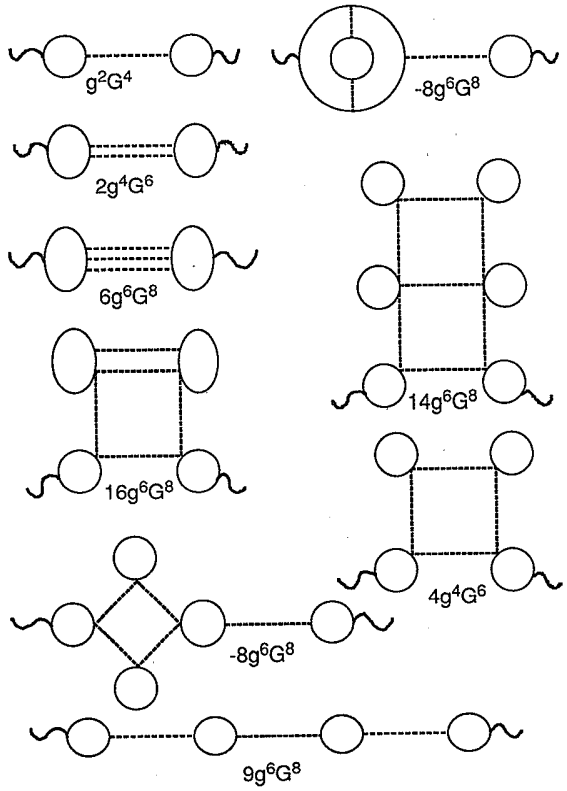

FIG. 12. Feynman diagram expansion of the correlation function C_{2a} of Fig. 11(a) using the Green's function and interaction vertices of Fig. 8. All graphs to order g^6 have been included.

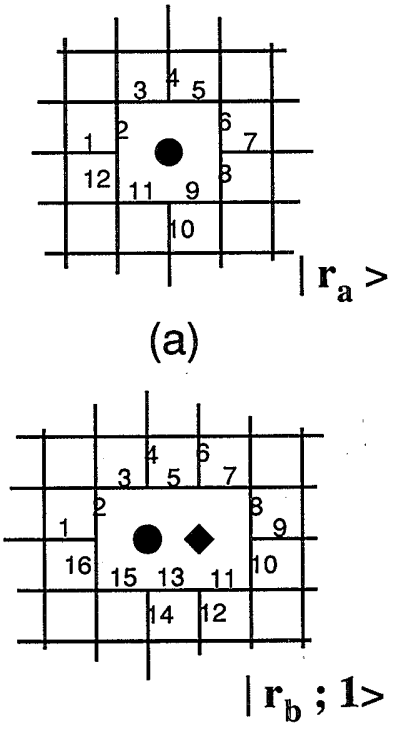

FIG. 13. The states $|\mathbf{r}_a\rangle$ and $|\mathbf{r}_b;1\rangle$ of Fig. 5. Some of the bonds have been numbered to identify the $g_a(i,j)$ and $g_{b1}(i,j)$ parameters on them.

$$C_{5a}=0g^6G^{11},\quad C_{5b}=2g^6G^{11}\ , \tag{A17}$$

and six-point functions,

$$C_6=2g^6G^{12}\ . \tag{A18}$$

The ground-state energy and the sublattice magnetization can now be calculated from the expressions in Eqs. (A4)–(A6); we use the decomposition the E correlation functions in Eqs. (A8)–(A13) and the values of the connected C correlation functions in Eqs. (A14)–(A18). The results of such a calculation and the subsequent minimization of the energy as a function of g are summarized in Table II.

APPENDIX B

This appendix presents the results of the evaluation of the matrix elements of the Hamiltonian H_h for wave function I. The matrix elements for wave function II can be evaluated in a very similar manner, with however, a much larger number of parameters.

The states we are considering are redrawn in Fig. 13. For simplicity we will allow the $g_a(i,j)$ and $g_{ba}(i,j)$ parameters to differ from their values at infinity only on the bonds that been numbered in Fig. 13. This is done simply to make the following discussion compact; the results of the paper were obtained in a calculation in which much larger sets of the $g_a(i,j)$ and $g_{ba}(i,j)$ parameters were allowed to vary. The numbers on the bonds are used to represent the variational parameters; the variational parameters are therefore $g_a(1)$, $g_a(2)\cdots g_a(12)$, $g_{b1}(1)$, $g_{b1}(2)\cdots g_{b1}(16)$, and similarly for g_{b2}, g_{b3}, and g_{b4}, leading to a total of 78 variational parameters. We represent by the symbol $g\,(=\frac{1}{6})$ the values of the g_a and g_b parameters on all the other bonds of the lattice.

The following are the values of the diagonal matrix elements of H_h so obtained:

$$\begin{aligned}\langle \mathbf{r}_a|H_h|\mathbf{r}\rangle=&-\frac{NJ}{2}(1-g+3g^2)+J-J[g_a(1)+g_a(2)+g_a(3)+g_a(4)+g_a(5)+g_a(6)+g_a(7)\\&+g_a(8)+g_a(9)+g_a(9)+g_a(10)+g_a(11)+g_a(12)-16g]\\&+\frac{10J}{4}[g_a^2(1)+g_a^2(2)+g_a^2(3)+g_a^2(4)+g_a^2(5)+g_a^2(6)+g_a^2(7)+g_a^2(8)+g_a^2(9)\\&+g_a^2(10)+g_a^2(11)+g_a^2(12)-\tfrac{96}{5}g^2]\ ,\end{aligned} \tag{B1}$$

$$\begin{aligned}\langle \mathbf{r}_b;1|H_h|\mathbf{r}_b;1\rangle=&-\frac{NJ}{2}(1-g+3g^2)+\frac{5J}{2}-J[g_{b1}(1)+g_{b1}(2)+g_{b1}(3)+g_{b1}(4)+g_{b1}(5)\\&+g_{b1}(6)+g_{b1}(7)+g_{b1}(8)+g_{b1}(9)+g_{b1}(10)\\&+g_{b1}(11)+g_{b1}(12)+g_{b1}(13)+g_{b1}(14)+g_{b1}(15)+g_{b1}(16)-23g]\\&+\frac{J}{4}[10g_{b1}^2(1)+10g_{b1}^2(2)+10g_{b1}^2(3)+10g_{b1}^2(4)+6g_{b1}^2(5)\\&+8gg_{b1}^2(6)+8g_{b1}^2(7)+8g_{b1}^2(8)+8g_{b1}^2(9)+8g_{b1}^2(10)+8g_{b1}^2(11)+8g_{b1}^2(12)\\&+6g_{b1}^3(13)+10g_{b1}^2(14)+10g_{b1}^2(15)+10g_{b1}^2(16)-276g^2]\ ,\end{aligned} \tag{B2}$$

and similarly for $|\mathbf{r}_b;2\rangle$, $|\mathbf{r}_b;3\rangle$, and $|\mathbf{r}_b;4\rangle$.

The off-diagonal matrix elements arising from the hopping term displace the position of the hole. We denote the displacement of the hole by the vector (h_x,h_y), where h_x and h_y are integer lattice spacings. In this way we obtain

$$\begin{aligned}\langle \mathbf{r}_a|H_h|\mathbf{r}_b=\mathbf{r}_a+(-1,0);1\rangle=&-\frac{t}{2}\{2-g_a^2(1)-g_a^2(2)-g_a^2(12)-[g_a(3)-g_{b1}(5)]^2\\&-[g_a(4)-g_{b1}(6)]^2-[g_a(5)-g_{b1}(7)]^2-[g_a(6)-g_{b1}(8)]^2[-g_a(7)-g_{b1}(9)]^2\\&-[g_a(8)-g_{b1}(10)]^2-[g_a(9)-g_{b1}(11)]^2-[g_a(10)-g_{b1}(12)]^2\\&-[g_a(11)-g_{b1}(13)]^2-[g-g_{b1}(14)]^2-[g-g_{b1}(15)]^2-[g-g_{b1}(16)]^2\\&-[g-g_{b1}(1)]^2-[g-g_{b1}(2)]^2-[g-g_{b1}(3)]^2-[g-g_{b1}(4)]^2\}\ ,\end{aligned} \tag{B3}$$

$$\langle \mathbf{r}|H_h|\mathbf{r}_b=\mathbf{r}_a+(1,0);1\rangle=tg_a(7)\ , \tag{B4}$$

$$\langle \mathbf{r}_a|H_h|\mathbf{r}_b=\mathbf{r}_a+(0,1);1\rangle=tg_a(5)\ , \tag{B5}$$

$$\langle \mathbf{r}_a|H_h|\mathbf{r}_b=\mathbf{r}_a+(0,-1);1\rangle=tg_a(9)\ , \tag{B6}$$

and similarly for $|\mathbf{r}_b;2\rangle$, $|\mathbf{r}_b;3\rangle$, and $|\mathbf{r}_b;4\rangle$.

Finally, there are the matrix elements arising from the nonorthogonality of the $|\mathbf{r}_b;\alpha\rangle$ states. These are found to be

as follows (the convention for bond numbering in the $|\mathbf{r}_b;2\rangle$, $|\mathbf{r}_b;3\rangle$, and $|\mathbf{r}_b;4\rangle$ states is obtained by rotating the $|\mathbf{r}_b;1\rangle$ state anticlockwise for 90, 180, and 270°, respectively):

$$\begin{aligned}
&\langle \mathbf{r}_b;1|\mathbf{r}_b;2\rangle = g_{b1}(13)g_{b2}(5)\ , \\
&\langle \mathbf{r}_b;1|\mathbf{r}_b;4\rangle = g_{b1}(5)g_{b4}(13)\ , \\
&\langle \mathbf{r}_b;1|H_h|\mathbf{r}_b;2\rangle = J\{(-N/2+4)g_{b1}(13)g_{b2}(5) - \tfrac{1}{2}[g_{b1}(13)+g_{b2}(5)]\}\ , \\
&\langle \mathbf{r}_b;1|H_h|\mathbf{r}_b;4\rangle = J\{(-N/2+4)g_{b1}(5)g_{b4}(13) - \tfrac{1}{2}[g_{b1}(5)+g_{b4}(13)]\}\ ,
\end{aligned} \tag{B7}$$

and similarly for $|\mathbf{r}_b;2\rangle$, $|\mathbf{r}_b;3\rangle$, and $|\mathbf{r}_b;4\rangle$.

[1] J. G. Bednorz and K. A. Muller, Z. Phys. B **64**, 188 (1986); M. K. Wu *et al.*, Phys. Rev. Lett. **58**, 908 (1987).
[2] P. W. Anderson, Science **235**, 1196 (1987).
[3] G. Shirane, Y. Endoh, R. J. Birgeneau, M. A. Kastner, Y. Hidaka, M. Oda, M. Suzuki, and T. Murakami, Phys. Rev. Lett. **59**, 1613 (1987).
[4] S. Chakravarty, B. I. Halperin, and D. R. Nelson, Phys. Rev. Lett. **60**, 1057 (1988).
[5] D. A. Huse and V. Elser, Phys. Rev. Lett. **60**, 2531 (1988).
[6] J. D. Reger and A. P. Young, Phys. Rev. B **37**, 5978 (1988).
[7] J. C. Fisher, J. Phys. Chem. Solids **10**, 44 (1959).
[8] T. Eguchi, J. Phys. Chem. Solids **24**, 1049 (1963).
[9] C. M. Varma (private communication).
[10] D. A. Huse, Phys. Rev. B **37**, 2380 (1988).
[11] S. Liang, B. Doucot, and P. W. Anderson, Phys. Rev. Lett. **61**, 365 (1988).
[12] J. E. Hirsch, Phys. Rev. Lett. **54**, 1317 (1985).
[13] S. A. Trugman, Phys. Rev. B **37**, 1597 (1988).
[14] B. I. Shraiman and E. D. Siggia, Phys. Rev. Lett. **61**, 467 (1988).
[15] C. Kane, P. A. Lee, and N. Read, Phys. Rev. B (to be published).
[16] S. Schmitt-Rink, C. M. Varma, and A. E. Ruckenstein, Phys. Rev. Lett. **60**, 2793 (1988).
[17] B. I. Shraiman and E. D. Siggia, Phys. Rev. Lett. **60**, 740 (1988).
[18] G. A. Thomas *et al.*, Phys. Rev. Lett. **61**, 1313 (1988).
[19] T. Holstein and H. Primakoff, Phys. Rev. **58**, 1098 (1940).
[20] P. Jordan and E. Wigner, Z. Phys. **47**, 631 (1928).
[21] S. Samuel, J. Math. Phys. **21**, 2816 (1980); **21**, 2880 (1980).
[22] K. B. Lyons, P. A. Fleury, L. F. Schneemeyer, and J. V. Waszczak, Phys. Rev. Lett. **60**, 732 (1988).